



## ORIGINAL ARTICLE

# Design, synthesis, characterization of zirconium (IV), cadmium (II) and iron (III) complexes derived from Schiff base 2-aminomethylbenzimidazole, 2-hydroxynaphthaldehyde and evaluation of their biological activity

Ahmed N. Al-Hakimi <sup>a,b,\*</sup>, Fahad Alminderej <sup>a</sup>, Lotfi Aroua <sup>a,c,1</sup>, Sadeq K. Alhag <sup>d,e</sup>,  
Mohammad Y. Alfaifi <sup>i</sup>, Samir O. M <sup>f,g</sup>, Jazem A. Mahyoub <sup>h</sup>,  
Serag Eldin I. Elbehairi <sup>i,j</sup>, Abrar S. Alnafisah <sup>a</sup>

<sup>a</sup> Chemistry Department, College of Sciences, Qassim University, Qassim, Saudi Arabia

<sup>b</sup> Chemistry Department, College of Sciences, Ibb University, Ibb, Yemen

<sup>c</sup> Laboratory of Organic Structural Chemistry & Macromolecules, Department of Chemistry, Faculty of Sciences of Tunis, Tunis El-Manar University, El Manar I 2092, Tunis, Tunisia

<sup>d</sup> Biology Department, College of Science and Arts, King Khalid University, Muhayl Asser, Saudi Arabia

<sup>e</sup> Biology Department, College of Science, Ibb University, Ibb, Yemen

<sup>f</sup> Physics Department, College of Science, Ibb University, Ibb, Yemen

<sup>g</sup> Quality Assurance Deanship, Al-Janad University for Science & Technology, Taiz, Yemen

<sup>h</sup> Biology Department, College of Science and Arts, King Abdulaziz University, Jeddah, Saudi Arabia

<sup>i</sup> King Khalid University, Faculty of Science, Biology Department, Abha 9004, Saudi Arabia

<sup>j</sup> Cell Culture Lab, Egyptian Organization for Biological Products and Vaccines (VACSERA Holding Company), 51 Wezaret El-Zeraa St., Agouza, Giza, Egypt

Received 11 June 2020; accepted 14 August 2020

Available online 25 August 2020

## KEYWORDS

Schiff base complexes;  
2-Aminomethylbenzimidazole;

**Abstract** (*E*)-1-((((1*H*-benzo[d]imidazol-2-yl)methyl)imino)methyl)naphthalen-2-ol, ligand was synthesized by condensation of (1*H*-benzo[d]imidazol-2-yl) methanamine, with 2-hydroxynaphthaldehyde. The ligand and the metal complexes were characterized by various spectroscopic techniques. Interpretation of spectra confirmed that the ligand adopted either a neutral

\* Corresponding author at: Chemistry Department, College of Sciences, Qassim University, Qassim, Saudi Arabia.

E-mail addresses: [Alhakemi10@yahoo.com](mailto:Alhakemi10@yahoo.com), [A.Alhakimi@qu.edu.sa](mailto:A.Alhakimi@qu.edu.sa) (A.N. Al-Hakimi), [lm.aroua@qu.edu.sa](mailto:lm.aroua@qu.edu.sa) (L. Aroua).

<sup>1</sup> Coauthor.

Peer review under responsibility of King Saud University.



Production and hosting by Elsevier

Potential anticancer colon agents;  
Antimicrobial;  
Insecticide agents

tridentate or a monobasic tridentate mode, bonded to the metal ions through the nitrogen atom of the heterocyclic benzimidazole, azomethine nitrogen atom and deprotonated phenolic oxygen atom forming either a square planer geometry. X-ray powder diffraction analysis of complexes indicated that the complexes were crystalline in nature with triclinic structures. The antibacterial and the antifungal activities of the ligand and its complexes were examined against *Escherichia coli*, *Bacillus subtilis* and *Aspergillus niger* by well-diffusion method. The results showed that Cd (II) complex exhibits the highest antifungal and antibacterial activities among the tested complexes. The in vitro antitumor activities of the different complexes were tested and the results revealed an important cytotoxicity of cadmium complex against MCF-7, Hep G2 and HCT 116 cell. Iron complex showed also a strong toxicity towards Hep G2 and HCT cell whereas moderate activity against MCF-7. The bioassay study of different complexes against mosquito larvae demonstrated strong activity of zirconium complex with 0.172 values of LC50.

© 2020 The Authors. Published by Elsevier B.V. on behalf of King Saud University. This is an open access article under the CC BY-NC-ND license (<http://creativecommons.org/licenses/by-nc-nd/4.0/>).

## 1. Introduction

Target benzimidazole compounds represent one of the heterocyclic classes owning a multitude of biological activity and clinical therapy. Benzimidazole derivatives are used for bioactivity in the treatment for various diseases including antibacterial (Eman et al., 2020), antifungal (Chandrika et al.; 2016, Leila et al., 2020), anti-tuberculous (Vatsal et al., 2020; Gill et al., 2008), antimalarial (Rudolf et al., 2020), analgesic and anti-inflammatory (Maghraby et al., 2020; Monika et al., 2014), anti-amoebic (Balasubramanian et al., 2012), and anti-histamine (Wang et al., 2012). Some benzimidazole was employed as antiplasmodial agents (Rylands et al., 2019) and have an insecticidal activity (Arfa et al., 2015).

In addition, current progress on substituted benzimidazoles exhibited diverse heterocycles at 2-position to generate potent anticancer agents at multiple carcinoma cell lines. These cover pyrimidine derivatives (Yadav et al., 2016), pyrazoline derivatives (Shaharyar et al., 2010), and thiazole derivatives (Luo et al., 2011). Furthermore, 2-substituted benzimidazoles possessed chloro or carboxy group at 5-position linked with 4-amino-thioxothiazole, 4-oxothiazolidine, 4-fluorobenzylidene and cycloalkylidene reviewed as potent antitumor agents (Refaat, 2010).

Later, all surveys motivated scientists to discover a new molecular architecture possessing significant biological activity (Osipyan et al.). Indeed, the benzimidazoles have numerous uses, especially, widely applied as ligands in the preparation of metal complex. A variety of studies on benzimidazole complexes that revealed a diverse and important biological activity including antiamoebic (Neelam et al., 2000), inhibition of protein tyrosine phosphatases (Ying et al., 2011), antiproliferative agents (Ying et al., 2011), antibacterial (Fahd, 2020; Lotfi, 2020), antimalarial (Patricia et al., 2013), and anticancer (Ülku et al., 2019).

On the other hand, complexes derived from 2-aminomethylbenzimidazole were well documented which represent one of the most target compounds that have multiple biological activities in medicinal and pharmacological fields (Abeer et al., 2015). Miscellaneous reports mentioned the good efficiency of 2-aminomethylbenzimidazole complexes against cancer cell in particular cytotoxic activity on MCF-7 cell line (Fatma et al., 2003), colon carcinoma (HCT116) and larynx carcinoma (HEP2) (Ahmed, 2011), hepatocellular carcinoma

(HepG2) and neuroblastoma (SHSY5Y) (Maurício et al., 2019).

Recently, Naeema et al. described the synthesis Schiff base metal complexes of Co(II), Ni(II), Cu(II) and Zn(II) derived from 2-aminomethylbenzimidazole and 2-hydroxynaphthaldehyde (Naeema et al., 2017).

This article describes the synthesis of Schiff base from 2-aminomethyl benzimidazole and 2-hydroxynaphthaldehyde as a ligand. Three different metal chlorides were prepared, including ZrCl<sub>4</sub>, CdCl<sub>2</sub>·6H<sub>2</sub>O, and FeCl<sub>3</sub>·6H<sub>2</sub>O. This work aims to assess the biological activity of synthesized compounds. First, all complexes were tested against colon cancer cells. Second, the antibacterial activity was assayed against *Escherichia coli* and *Bacillus subtilis*. The antifungal activity using Fungus (*Aspergillus niger*) was reported here. Finally, the ligand and its complexes were also tested as insecticide agents.

## 2. Experimental section

### 2.1. Materials and methods

FT-IR spectroscopy was recorded using Thermo-Nicolet-6700 FT-IR spectrometer by the KBr disc technique in the wavenumber range of 4000–400 cm<sup>-1</sup>. Electronic absorption spectral was carried out in DMF on a UV-2102 PC Shimadzu spectrophotometer using 1 cm matched quartz cell in the wavelength range 200–900 nm. The <sup>1</sup>H NMR and <sup>13</sup>C NMR were recorded on Bruker NMR at 400 MHz and 100 MHz, respectively. The chemical shifts were measured with reference to TMS as internal standard in deuterated DMSO as the solvent. Simultaneous TGA and DTA analyses were performed employing a Shimadzu DTG-60 instrument using a heating rate of 10 °C / min in air atmosphere. The average samples weight was 10 mg α-Al<sub>2</sub>O<sub>3</sub> and used as a reference material in the DTA measurements. The X-ray powder diffraction patterns of the compounds were recorded using XRD diffractometer Model PW 1710 control unit (Philips). The anode material was Cu Kα (λ = 1.54180 Å) and operated at 40 K.V and 30 M.A. The mass spectra of the different complexes were registered in a positive mode using the DART-ToF-MS. The most intense fragment ions resulting from cleavage possible from the compounds detected were chosen and analyzed. The high-resolution mass spectrometer instrument

used was AccuTOF LC-Plus from JEOL (Japan). All reagents employed in the synthesis of different complexes were commercially available without purification. 2-aminomethylbenzimidazole was purchased from Sigma-Aldrich.

## 2.2. Preparation of ligand ( $H_2L$ ) (1).

The ligand was prepared by common method (Nacema et al., 2017). Yield (75%). m.p. 126 °C. EI-MS spectra  $m/z$  = 301. IR (KBr),  $\nu$  ( $cm^{-1}$ ): 3420 (s, br), 3255(s), 1631(s), 1548(m), 1320 (m).  $^1H$  NMR (300 MHz, DMSO  $d_6$ )  $\delta$  (ppm):  $\delta$ : 5.07(s, 2H,  $CH_2$ ), 6.77–8.09(d, m, 10H, Ar-H), 9.29 (s, 1H, N=CH), 12.66 (s, 1H, NH imidazole), 14.16 (d, 1H, ArOH).  $^{13}C$  NMR (125 MHz, DMSO  $d_6$ )  $\delta$  (ppm): 175.68, 161.46, 151.06, 138.01, 134.61, 134.17, 129.48, 128.76, 126.3, 124.57, 123.39, 119.25, 119.03, 112.02, 106.99, 50.09, UV-Vis (DMF);  $\lambda_{max}$  (nm): 272, 318, 420.

## 2.3. Preparation of the metal complexes

Metal complexes were prepared by mixing a hot ethanolic solution of the metal salts:  $ZrCl_4$ ,  $CdCl_2 \cdot 6H_2O$  and  $FeCl_3 \cdot 6H_2O$  with a suitable amount of a hot ethanolic solution of the ligand in molar ratio 1 M:1 L (metal:ligand). The reaction mixture was refluxed 3 h under reflux. At the end of reaction, the reaction mixture was filtered. The formed precipitates were washed with ethanol and then with diethyl ether and finally dried under vacuum over anhydrous  $CaCl_2$ .

### 2.3.1. Zirconium complex $Zr(IV)$ (2)

Orange precipitate; Mp: 310 °C, yield (78%), UV-Vis (DMF);  $\lambda_{max}$  [nm]: 282; 350. IR (KBr,  $\nu$  / $cm^{-1}$ ): =, 3260 (m), 1600 (m), 1554 (m), 1325 (m), 661(m), 551 (s), 450 (m). HRMS (DART-TOF-MS, positive mode)  $m/z$  = 434.25890, 386.22732, 330.16139, 296.1904, 267.1574, 211.09619, 189.13845.

### 2.3.2. Cadmium complex $Cd(II)$ (3)

Red precipitate, yield (80%), Mp: 190 °C, UV-Vis (DMF),  $\lambda_{max}$  (nm): 282. IR (KBr),  $\nu$  ( $cm^{-1}$ ): = 3261 (m), 1615 (m), 1550(m), 1307 (s), 594 (s), 547(m), 454 (m). HRMS (DART-TOF-MS, positive mode)  $m/z$  = 448.19515, 395.19103, 370.17865, 336.21198, 314.13062, 293.15230, 261.10118, 283.13390, 186.09159, 161.11262, 133.07561, 108.04600.

### 2.3.3. Iron complex $Fe(III)$ (4)

Dark precipitate, yield (75%), Mp: 280 °C, UV-Vis (DMF),  $\lambda_{max}$  (nm): 282. IR (KBr),  $\nu$  ( $cm^{-1}$ ): = 3430(s), 3290 (m), 1620(m), 1590 (m), 1300 (s), 661 (s), 580(m), 440 (s). HRMS (DART-TOF-MS, positive mode)  $m/z$  = 393.17835, 314.13699, 261.10030, 238.13376, 211.09752, 196.08782.

## 2.4. Cell culture

Cell lines, human breast adenocarcinoma (MCF-7), hepatocellular carcinoma (HepG-2) and colorectal adenocarcinoma (HCT 116) were received from the American Type Culture Collection (ATCC). Cells were preserved in RPMI-1640 supplemented with (100  $\mu g/mL$ ), penicillin (100 units/ mL) and heat-inactivated fetal bovine serum (10% v/v) in a humidified,

5% (v/v)  $CO_2$  atmosphere at 37 °C (Ali Mokhtar et al., 2012; Sabrin et al., 2016).

## 2.5. Cytotoxicity assay

Cells were treated with six various concentrations of each complexes (0.01, 0.1, 1, 10, 100 and 1000  $\mu g$ ); untreated cells (control) were added. The cells were incubated with each concentration for 72 h and finally fixed with TCA (10% w/v) for 1 h at 4 °C. Cells were washed several times and stained by 0.4% (w/v) SRB solution for 10 min in a dark place. The excess of stain was extracted and eliminated with 1% (v/v) glacial acetic acid. The SRB-stained cells were dried overnight, then dissolved with Tris-HCl and the color intensity was analyzed in a microplate reader at 540 nm. The relation between viability percentage of each tumor cell line and compound concentrations was analyzed to get the IC50 (dose of the drug which reduces survival to (50%)) using Sigma Plot 12.0 software (Jeong-Chae et al., 2002).

## 2.6. In-vitro antimicrobial and antifungal activity

All tests of antimicrobial and antifungal activities for the compounds (ligand and complexes) were achieved in the Botany Department, Laboratory of microbiology. The antimicrobial activities of the compound were studied by Well Diffusion Method (Abdulrahman et al., 2018). The antibacterial activities were examined using *E. coli* and *B. subtilis*, while the antifungal activity was achieved using Fungus (*A. niger*) in DMSO, and poured disc was used as a negative control. The resulting wells are sites for tested compounds of known concentration. For comparison, a standard antibacterial drug (tetracycline), an antifungal drug (nystatin) as a positive control. A solution of metal salts was also examined under similar conditions. Areas of growth inhibition around the holes were observed, which indicates that the tested compound inhibits the growth of microorganisms. The zone of inhibition was carefully measured in millimeters. All determinations were made in triplicate for each compound. An average of the two independent readings for each compound was recorded.

## 2.7. Rearing of mosquitoes

The mosquitoes in the south of the house (*Aedes aegypti*) were transferred to the Dengue Mosquito Station, Jeddah, for rearing. During the rearing, the mosquito larvae produced were introduced into plastic enamel trays containing tap water. The rearing conditions were fixed at ( $27 \pm 2$  °C) and 75–78% RH with photoperiod (14:10 light and dark) respectively. A special diet for mosquitoes was prepared from brewer's yeast, dog biscuits and algae taken from pond water in a ratio of 3: 1: 1, respectively Gerald (Gerald et al., 1996).

## 2.8. Larvicidal activity of four chemical compounds

Amid initial screening with the lab experiment, *A. aegypti* mosquito's larvae were collected, identified, from the rearing cage at dengue station, King Abdulaziz University, Jeddah. From the stock solution with the use of dechlorinated tap water 1000 mg/l extract was prepared. This material was received

from the World health organization with slight modifications (Abdul et al., 2000).

### 3. Results and discussion

#### 3.1. Chemistry

Our approach started with the synthesis of the ligand by reacting one equivalent ethanolic solution of 2-aminomethylbenzimidazole (AMBI) with one equivalent ethanolic solution of 2-hydroxynaphthaldehyde according to Fig. 1. The synthesis of the complexes were achieved by reacting one equivalent ethanolic solution of Ligand ( $H_2L$ ) with one equivalent of metal chloride salt ( $ZrCl_4$ ,  $FeCl_3 \cdot 6H_2O$  and  $CdCl_2 \cdot 6H_2O$ ) inside the same solvent ethanol (Fig. 2). The reaction initiated by reacting 8.4 m.mol of metal halides solution with 8.4 m.mol solution of Ligand ( $H_2L$ ) at room temperature. The mixture was heated gradually and left under reflux for 3 h (Table 1).

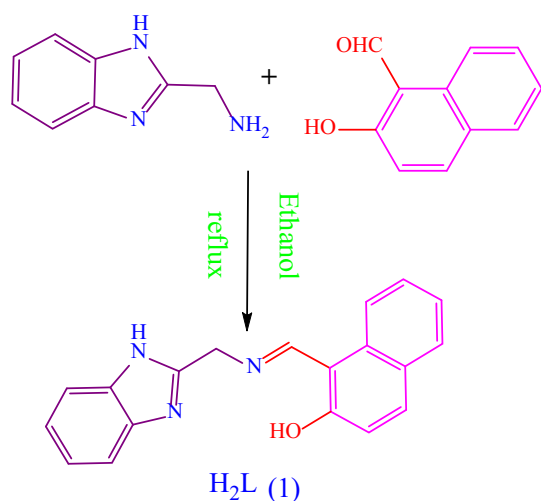


**Fig. 1** Synthesis of ligand ( $H_2L$ ) (E)-1-(((1H-benzo[d]imidazol-2-yl)methyl)imino)methylnaphthalen-2-ol.

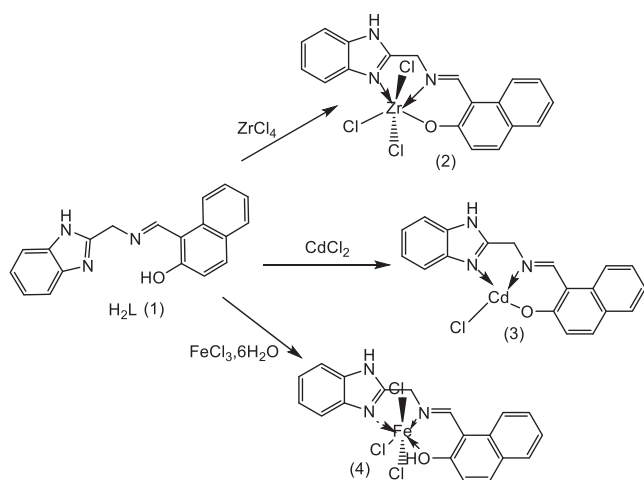


**Fig. 2** Structures of complexes Co (II), Cd(II) and Fe(III).

All obtained complexes were characterized by spectroscopic data of FT-IR, high resolution mass spectrometry (HRMS), UV-Visible electronic absorption, thermal analysis and X-ray powder diffraction studies.

#### 3.1.1. Mass spectra

The mass spectrum of the zirconium complex illustrated in Fig. 3, manifest the absence of molecular peak. This structure was proved essentially by ion peak situated at  $m/z = 434,2589$  (calcd.: 433,91658) corresponding to methyl-5-vinylimidazolmethylene azanylidene methylphenol linked to zirconium metal and three chlorine atoms. The fragment at  $m/z = 386.22732$  (calcd. 385,91658) was attributed to hydroxybenzylideneamino-N-methyl acetimidamide connected to zirconium metal and three chlorine atoms. Furthermore, the spectra revealed the presence of basic peak at  $m/z = 211,09619$  (calcd. 210,95692) assigned to 2-aminomethylphenol linked to zirconium metal. These data confirmed that the zirconium is linked with ligand via oxygen atom and coordinated with the azomethine group of both benzimidazole group and Schiff base motif (Fig. 3).

Regarding the iron complex, the mass spectrum illustrated in Fig. 4, manifest the absence of molecular ion peak. The structure was also confirmed by the fragment at  $m/z = 393,17835$  (calcd. 393,03258) corresponding to the loss of two chlorine atoms from the molecular mass ion. The fragment at  $m/z = 314,13699$  (calcd. 314,09503) was attributed to benzimidazol methylaminomethylcyclohexanol connected to iron metal. The basic fragment at  $m/z = 261,10030$  (calcd. 261,05591) was associated with 4,5-dihydroimidazol methylaminomethylphenol joined with iron metal. The structure was also confirmed with the fragment at  $m/z = 238,13376$  (calcd. 237,98289) related to aminomethylbenzimidazole linked with iron metal and a chlorine atom. These results proved the formation of the complex and possess a hexagonal structure described above proposes that the coordination of the iron was provided by the hydroxyl OH group and also with both azomethine groups (Fig. 2).

The structure of the Cd (II) complex was established by mass spectrometry data and suggests tetrahedral coordination with ligand. The mass spectrum of the cadmium complex, reported in Fig. 5, affirmed the presence of a molecular ionic peak  $(M-H)^+$  at  $m/z = 448,19515$  (calcd. 447,97752). The structure was proved by the basic fragment at  $m/z = 261,10118$  (calcd. 260,98246) corresponding to 2-aminomethylbenzimidazole linked with cadmium. The fragment at  $m/z = 283,31390$  (calcd. 282,95557) was associated to (2-hydroxynaphthalen-1-yl) methaniminium attached with cadmium metal. The peak fragment at  $m/z = 238,13390$  (calcd. 238,00286) was attributed to hexahydro-1H-benzoimidazolium connected to cadmium metal. The fragment at  $m/z = 108,04600$  (calcd. 108,06820) was assigned to *o*-phenyldiamine motif.

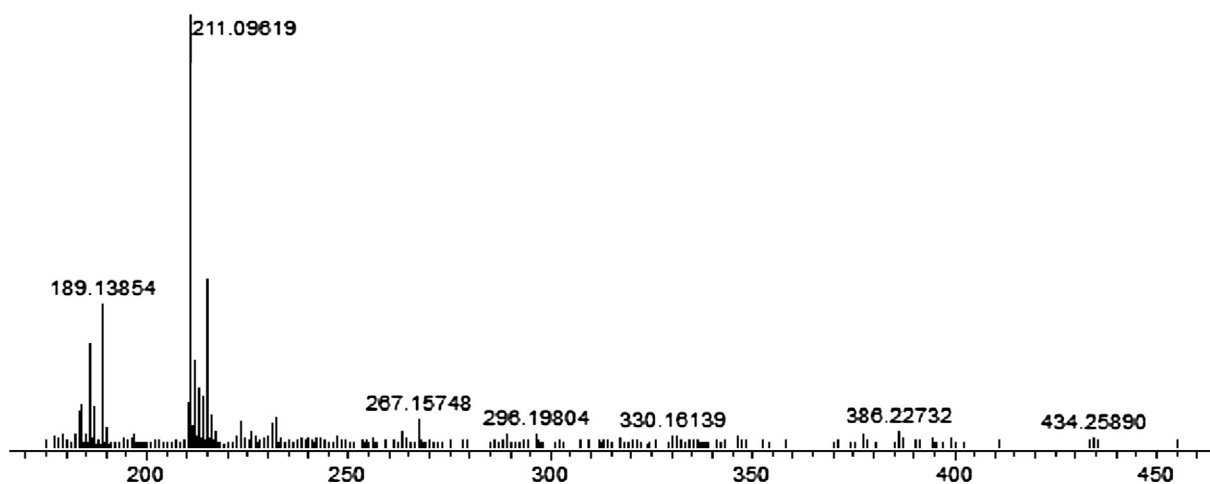
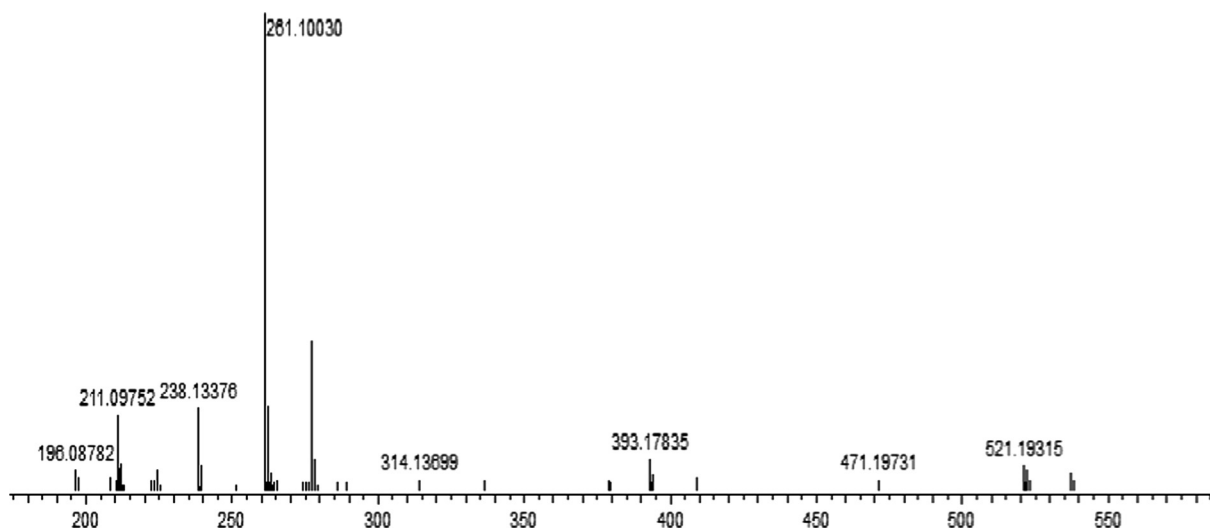
These data, in the case of the cadmium complex, confirmed that the metal is linked by the hydroxyl group of ligand and the coordination of cadmium metal was established by the azomethine groups.

#### 3.1.2. Electronic spectra

The Ultraviolet-visible (UV-Vis) absorption of ligand and its metal complexes were achieved in DMF at room temperature

**Table 1** Analytical data and Electronic data of ligand and their metal complexes.

Compound	Colour	Yield (%)	Mp(°C)	$\lambda_{\max}$ [nm]	$\nu(\text{Cm}^{-1})$	Assignment	
1	C <sub>19</sub> H <sub>15</sub> ON <sub>3</sub>	Yellow	80	272	36,764	$\pi \rightarrow \pi^*$	
				318	31,446	$n \rightarrow \pi^*$	
				420	23,809	$(\nu_2) {}^3A_2g(F) \rightarrow {}^3T_1g(F)$	
2	C <sub>19</sub> H <sub>14</sub> ON <sub>3</sub> ZrCl <sub>3</sub>	Orange	85	340	282	$\pi \rightarrow \pi^*$	
					350	29,411	LMCT
3	C <sub>19</sub> H <sub>14</sub> ON <sub>3</sub> CdCl	Red brick	80	280	282	$\pi \rightarrow \pi^*$	
					390	25,641	$n \rightarrow \pi^*$
4	C <sub>19</sub> H <sub>15</sub> ON <sub>3</sub> FeCl <sub>3</sub>	Dark Broun	75	190	530	${}^6A_{1g} \rightarrow {}^4T_{2g}$	
					480	20,833	${}^6A_{1g} \rightarrow {}^4T_1(G)$
					410	24,390	${}^6A_{1g} \rightarrow {}^4E_g(G)$
					282	35,460	$\pi \rightarrow \pi^*$

**Fig. 3** Mass Spectra of Zr (IV) complex.**Fig. 4** Mass Spectra of Fe (III) complex.

and the results were written in Table 1. Free ligand (H<sub>2</sub>L) revealed, respectively, three transitions at 272 nm attributed to  $\pi \rightarrow \pi^*$  band, the second transition at 318 nm relatively

to  $n \rightarrow \pi^*$  band and the third transition at 420 nm associated to  $(\nu_2) {}^3A_2g(F) \rightarrow {}^3T_1g(F)$ . The energy of the ligand indicates that the difference between HOMO and LUMO is called the

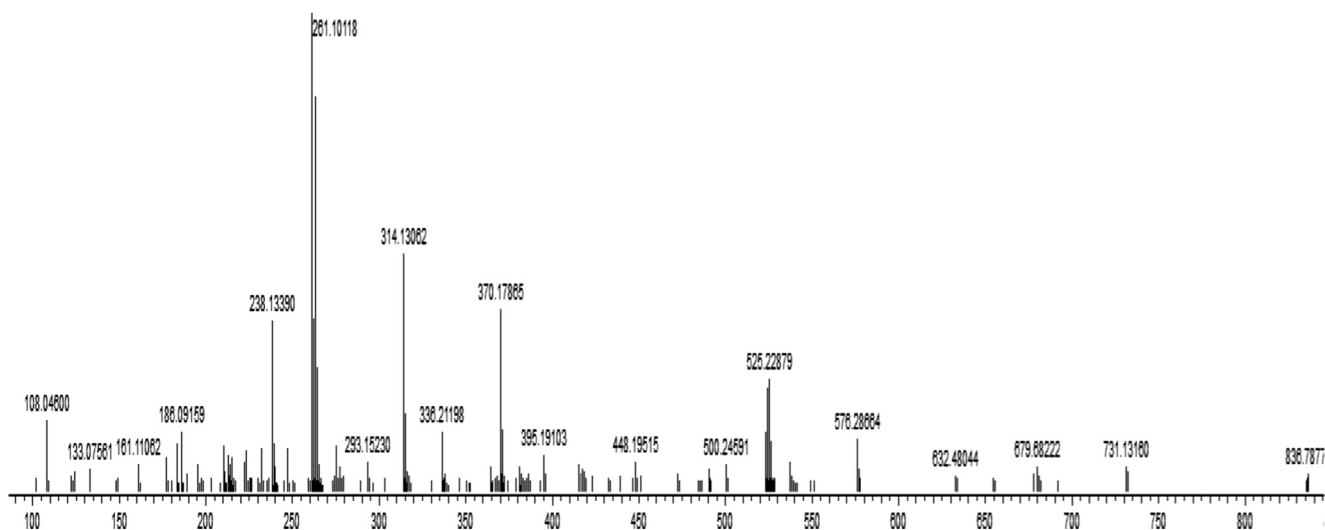


Fig. 5 Mass Spectra of Cd (II) complex.

HOMO-LUMO gap. In our case, this difference in energy between these two boundary orbitals referred to predict the strength and stability of transition metal complexes and the created bonds in compounds. The numerous of double and single bonds as well as nonbinding electrons represent an electron density in the ligand. This electron density makes the ligand effective for the correlation, interaction or very high vital. zirconium (IV) complexes (**2**) do not show d-d transitions. The bands observed in the 282, 350 nm may be due to intra-ligand transition and (LMCT) (Har and Jangbhadur, 2013).

Moreover, the cadmium (II) complex revealed the absence of d-d transition and except two transitions at 390 and 282 nm, it is assumed to  $\pi \rightarrow \pi^*$  and  $n \rightarrow \pi^*$  bands that confirmed the formation of the complex via the coordination of ligands to metal.

The iron (III) complex (**3**) provided four bands at 520, 460, 400 and 282 nm which assigned to  ${}^6A_{1g} \rightarrow {}^4T_{2g}$ ,  ${}^6A_{1g} \rightarrow {}^4T_1(G)$ ,  ${}^6A_{1g} \rightarrow {}^4E_g(G)$  and  ${}^6A_{1g} \rightarrow {}^4A_{1g}(G)$ , transitions. These bands characterize the octahedral iron (III) complex (El-Tabl et al., 2008a, 2008b).

### 3.1.3. IR spectra

Ligand has three possible sites for binding to the metallic element, namely the nitrogen of the azomethine group, oxygen of the hydroxyl group, and the nitrogen atom of the benzimidazole moiety. Therefore, the ligand can act as neutral or mono basic tridentate ion or non-ionic tridentate. In complexes (**2**) and (**3**) the ligand acts as a mono basic tridentate chelator forming two successive six and five rings. This behavior was confirmed by the negative shift in the position of the both azomethine and benzimidazole and the disappearance of the absorption peak of the hydroxyl group. Whereas in complex (**4**), the ligand behavior a neutral tridentate with metal forming six and five rings. This behavior was confirmed by the negative shift in the position of the both the azomethine, benzimidazole and the hydroxyl group.

The IR spectrum of the ligand  $H_2L$  was employed as reference in particular to compare the spectra of metal complexes. As presented in Table 2, the IR spectrum of the ligand exhib-

ited broad and strong features at  $3420\text{ cm}^{-1}$  attributed to the stretching vibration of the phenolic hydroxyl group. Inversely, the spectra of complexes (**2**) and (**3**) display the absence of the OH stretching vibration which corresponding to the deprotonation of the hydroxyl group in the formation processes of the complexes (**2**) and (**3**) whereas the medium band at  $3255\text{ cm}^{-1}$  may be assigned to  $\nu(\text{NH})$  group. The relatively strong and medium bands which located at  $1631$  and  $1570\text{ cm}^{-1}$  corresponded to the azomethine group (Ahmed, 2020; El-Tabl et al., 2008a, 2008b). In complexes (**2**) and (**3**) showed the ligand  $H_2L$  acts as a mono-negative tridentate O, N,N ligand coordinating via azomethine nitrogen ( $\text{C}=\text{N}$ ) and deprotonated phenolic hydroxyl group. This mode of bonding is supported by the disappearance of the band characteristic to hydroxyl group  $\nu(\text{OH})$  with simultaneous positive shift of  $\nu(\text{C}-\text{O}$  phenolic) band; the negative shift of azomethine group  $\nu(\text{C}=\text{N})$  band. This mode of chelation is supported by the appearance of new bands in the  $(661\text{--}584)\text{ cm}^{-1}$ ,  $(551\text{--}547)\text{ cm}^{-1}$  and  $(450\text{--}444)\text{ cm}^{-1}$  assigned to  $\nu(\text{M} \leftarrow \text{O})$ ,  $\nu(\text{M} \leftarrow \text{N})$  and  $(\text{M} \leftarrow \text{Cl})$  respectively (Table 2).

On the other hand, complex (**4**) manifest an absorption band at  $3425\text{ cm}^{-1}$  attributed to the stretching vibration of the phenolic hydroxyl group coordinated with iron (III) ion. The absorption bands of the coordinated nitrogen in both benzimidazole and azomethine group is located at  $3290\text{ cm}^{-1}$  and  $1626\text{ cm}^{-1}$ , respectively. This mode of chelation also is supported by the appearance of new bands in the  $661\text{ cm}^{-1}$ ,  $580\text{ cm}^{-1}$  and  $440\text{ cm}^{-1}$  assigned to  $\nu(\text{M} \leftarrow \text{O})$ ,  $\nu(\text{M} \leftarrow \text{N})$  and  $(\text{M} \leftarrow \text{Cl})$ , respectively.

### 3.1.4. Thermal analyses (DTA and TGA)

The DTA and TGA curves in the temperature range  $27\text{--}600\text{ }^\circ\text{C}$  for the complexes (**2**)–(**4**) emphasized that these complexes were thermally stable up to  $100\text{ }^\circ\text{C}$ . The change happened when the temperature rose to  $150\text{ }^\circ\text{C}$ , here the chlorine was released in the form of hydrochloride.

Complex (**2**) showed the decomposition peak at  $(250\text{--}300)\text{ }^\circ\text{C}$  with a mass loss  $21.50\%$  (Calcd.  $21.38\%$ ), corresponding to the loss of three hydrochloride. However, the spectra of complex (**2**) revealed a peak at  $550\text{ }^\circ\text{C}$  with mass loss

**Table 2** The IR spectral assignment for the ligand H<sub>2</sub>L and its metal complexes.

No.	Ligand/complexes	$\nu(\text{OH})$	$\nu(\text{NH})$	$\nu(\text{C}=\text{N})$	$\nu(\text{C}-\text{O})_{\text{ph}}$	$\nu(\text{M}-\text{O})$	$\nu(\text{M}-\text{N})$	$\nu(\text{M}-\text{Cl})$
1	C <sub>19</sub> H <sub>15</sub> N <sub>3</sub> O (H <sub>2</sub> L)	3420	3255	1631, 1570	1320	—	—	—
2	C <sub>19</sub> H <sub>14</sub> ON <sub>3</sub> ZrCl <sub>3</sub>	—	3260	1600,1550	1325	661	551	450
3	C <sub>19</sub> H <sub>14</sub> ON <sub>3</sub> CdCl	—	3361	1630,1555	1327	584	547	444
4	C <sub>19</sub> H <sub>15</sub> ON <sub>3</sub> FeCl <sub>3</sub>	3425 (br)	3290	1626,1560	1320	661	580	440

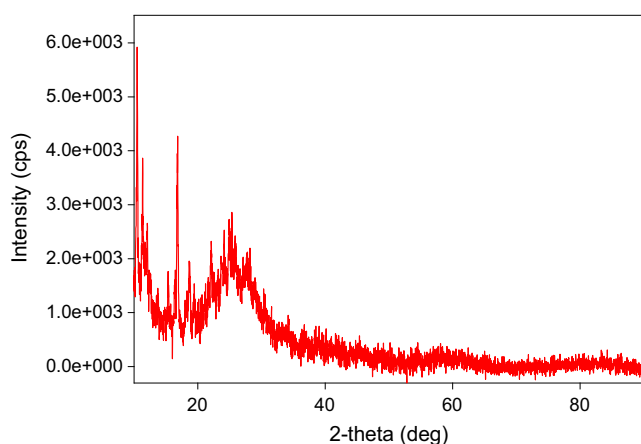
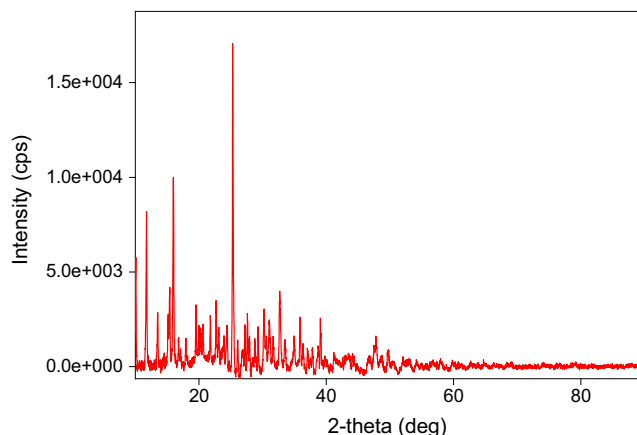
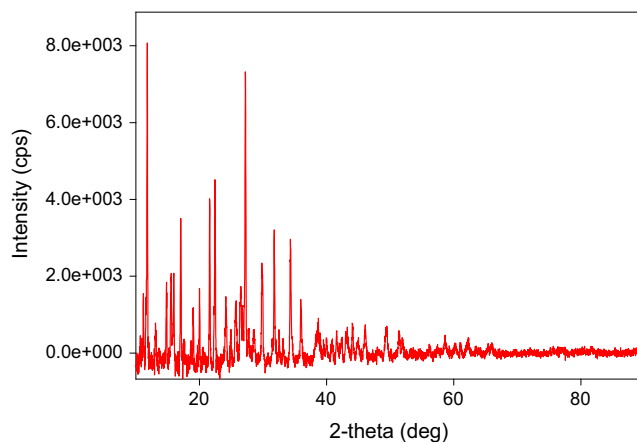
32.00% (Calcd. 31.46%), referring to the formation of ZrO<sub>2</sub>. Complex (3) exhibited an endothermic peak at 230 °C with a mass loss of 8.20% (Calcd. 8.15%), denoting the loss of one hydrochloride. In addition to the above, the observed peak at 550 °C with a mass loss 31.01% (Calcd. 31.21) referred to the formation of CdO.

The decomposition of iron complex (4) occurred at 270 °C with a mass loss 23.20% (Calcd. 23.07%) and this attributed to the elimination of three chloride ions. Also, the observed peak at 580 °C with a mass loss 49.21% (Calcd. 49.08) pointed to the formation of Fe<sub>2</sub>O<sub>3</sub>.

### 3.1.5. XRD analysis

The X-ray powder diffraction patterns of the three complexes are shown in Figs. 6-8. The output data from XRD measurements were treated and refined using some software. There are many computer codes that have been used to analyze the X-ray line profile. The residual-peak fitting (PeakFit) software was used. This program helps to detect, separate, quantify hidden peaks that standard instrumentation misses and background correction. PeakFit also includes different nonlinear spectral application line shapes (Singh et al., 2011).

A standard cell parameter was used for the three complexes as starting values for “CHEKCELL” program to identify the Bragg reflections (Karelle et al., 2018). CHEKCELL program is a powder Indexing software. The crystal lattice parameters were computed with the aid of the computer program CHEKCELL (Laugier et al., 2004). The crystal data of these complexes were observed and fitted well with the triclinic crystal system. The unit cell parameters of the complexes are given in Table 3. The different values of the calculated unit cell volumes are due to the sizes of impurities entered the base material. So, the large atom/molecule size will increase the cell unit

**Fig. 6** XRD Spectra of Zr (IV) complex.**Fig. 7** XRD Spectra of Cd (II) complex.**Fig. 8** XRD Spectra of Fe (III) complex.

volume and this leads to deformation in bonds as well as changing the properties of the product material.

Furthermore, using the diffraction data, the mean crystallite sizes of the complexes,  $D$ , were determined according to the Scherrer equation: ( $D = 0.9\lambda/(\beta\cos\theta)$ ), where  $\lambda$  is X-ray wavelength (1.54180 Å),  $\theta$  is Bragg diffraction angle, and  $\beta$  is the full width at half maximum of the strong diffraction peak of the samples (Miranda and Sasaki, 2018). The Fig. 7 show the crystalline nature of the three complexes and the peak sharpness in the XRPD patterns indicates the existence of the nano-sized complex. The average crystallite sizes of the three complexes are given in Table 3. The values of crystallite sizes indicate that Cd-complex is more crystalline than the others.

**Table 3** XRD data of Zr(IV), Cd(II) and Fe(II) complex.

Lattice and crystal parameters Zr(IV) complex							
a(Å)	b(Å)	c(Å)	$\alpha(^{\circ})$	$\beta(^{\circ})$	$\gamma(^{\circ})$	Cell Volume(Å <sup>3</sup> )	Crystal size nm
9.945	18.311	43.955	93.27	98.83	90.06	8255.73	22.99
Crystal type	Triclinic	Space group	P1				
Lattice and crystal parameters Cd(II) complex							
a(Å)	b(Å)	c(Å)	$\alpha(^{\circ})$	$\beta(^{\circ})$	$\gamma(^{\circ})$	Cell Volume(Å <sup>3</sup> )	Crystal size nm
7.869	14.695	13.756	89.93	102.36	90.54	1553.771	42.5
Crystal type	Triclinic	Space group	P1				
Lattice and crystal parameters Fe(II) complex							
a(Å)	b(Å)	c(Å)	$\alpha(^{\circ})$	$\beta(^{\circ})$	$\gamma(^{\circ})$	Cell Volume(Å <sup>3</sup> )	Crystal size nm
7.909	14.545	13.7568	90.44	102.01	90.22	1548.042	35.4
Crystal type	Triclinic	Space group	P1				

### 3.2. Biology

#### 3.2.1. In vitro antitumor activities

The in vitro cytotoxic activities of the tested compounds were determined using SRB assay towards MCF-7, HepG2 and HCT 116 tumor cell lines over concentration range of 0.01 to 1000 µg. Tested compounds showed variable cytotoxic activity against tumor human cells. It was observed that the most significant toxicity was with cadmium complex against MCF-7, HepG2 and HCT 116 cells with IC<sub>50</sub>s 5.1, 1.1 and 1.3, respectively. While the iron complex exhibited strong toxicity towards liver cancer (HepG2) among all compounds with IC<sub>50</sub> 0.4 µg. The iron complex was having potent toxicity against HCT 116 with IC<sub>50</sub> 1.4 µg and moderate effect towards breast cancer MCF-7 with IC<sub>50</sub> 19.5 µg (Fig. 9).

In addition, the ligand C<sub>19</sub>H<sub>15</sub>ON<sub>3</sub> (H<sub>2</sub>L) revealed a slight toxicity effect towards MCF-7 tumor cells with IC<sub>50</sub> 17.6 and moderate on HepG2 and HCT 116 cells with IC<sub>50</sub>s 5.7 and 10.2 µg, respectively. On the other hand, compound Zr (IV) Complex was weaker to kill cells of MCF-7, moderate with HepG2, and having a significant effect on HCT 116 with IC<sub>50</sub>s 45.6, 21.6 and 1.6 µg, respectively (Table 4).

#### 3.2.2. Antimicrobial activity

The biological activity of the ligand and its metal complexes were examined in vitro against two types of bacteria (*E. coli*), (*B. subtilis*) and one type of fungus (*A. niger*). The antimicrobial activities were expressed as a percentage of inhibition versus the standard drug, (Table 5). The results indicate a high efficacy of samples on bacteria and fungi. The ligand demonstrated high activity against all types of organisms. On the contrary, all-metal complexes showed promising activity against *E. coli*, and *B. subtilis*. On the other hand, the metal complexes demonstrated moderate activity against *A. niger*. Metal complexes were lower activity than the ligand due to increasing the polarity in metal ion (Fig. 10).

The fungicidal activity order of the complexes against *A. niger* was as follows: nystatin > Cd (II) complex > ligand (H<sub>2</sub>L) > Fe (III) complex > Zr(IV) Complex.

From another standpoint, the order of antibacterial activity for the different complexes against *B. subtilis* was as follows:

Tetracycline > Cd (II) complex = ligand (H<sub>2</sub>L) > Zr(IV) Complex > Fe (III) complex, and against *E. coli* was: Tetracycline > Cd (II) complex = ligand (H<sub>2</sub>L) > Zr(IV) Complex = Fe (III) complex.

#### 3.2.3. Bioassay against mosquito larvae

The results of the ligand (H<sub>2</sub>L) and their metal complexes manifested high larvicidal activity with low concentrations as stated in Tables 6 and 7. The relation between different concentrations and larvae death of these four compounds is illustrated in Fig. 11. The ligand (H<sub>2</sub>L) and cobalt complex revealed a high mortality rate of *A. aegypti* larvae at a concentration of 1 ppm. The cadmium and iron complex showed the highest activity at a concentration of 10 ppm and the mortality of larvae was 97.9 and 80.2, respectively.

The LC<sub>50</sub> value of the ligand (H<sub>2</sub>L), Zr(IV), cadmium (II), and iron (III) complexes were respectively 0.172, 0.309, 1.336, and 3.604 ppm, as illustrated in Fig. 11. These results proposed that ligand (H<sub>2</sub>L) and cobalt complex possess the ability to kill larvae of *A. aegypti* with low concentration. While at the same concentration for cadmium and iron complex, larvae were survived.

A comparative study was carried out and evaluated using five compounds against *A. aegypti*. The Given values of LC<sub>50</sub> (concentration: which kills 50 % of mosquito larvae) showed that the mosquito larvae of *A. aegypti* were more sensitive to Pesguard FG 161 (0.046 ppm) than to Actikil 50 % (0.061 ppm) and Bacilod (0.142 ppm), respectively. The results exhibited that Pesguard FG 161 was more effective against *A. aegypti* larvae than Actikil 50 % and Bacilod about 1.3 and 3.1 times, respectively (Deepak et al., 2014).

The comparative study of the larvicidal activity for the insecticides was tested against the larvae of *A. Aegypti*, and it demonstrated that the bacterial insecticide Bactilarvae was the most effective compound followed by OP Saftrotin, Temephos and Solfac (Samuel et al., 2012). Plant extracts showing larvicidal activity against *Culex quinquefasciatus* (Javaid et al., 2018).

**Conclusion:** In this paper, the synthesis of Schiff base elaborated from 2-aminomethylbenzimidazole and 2-

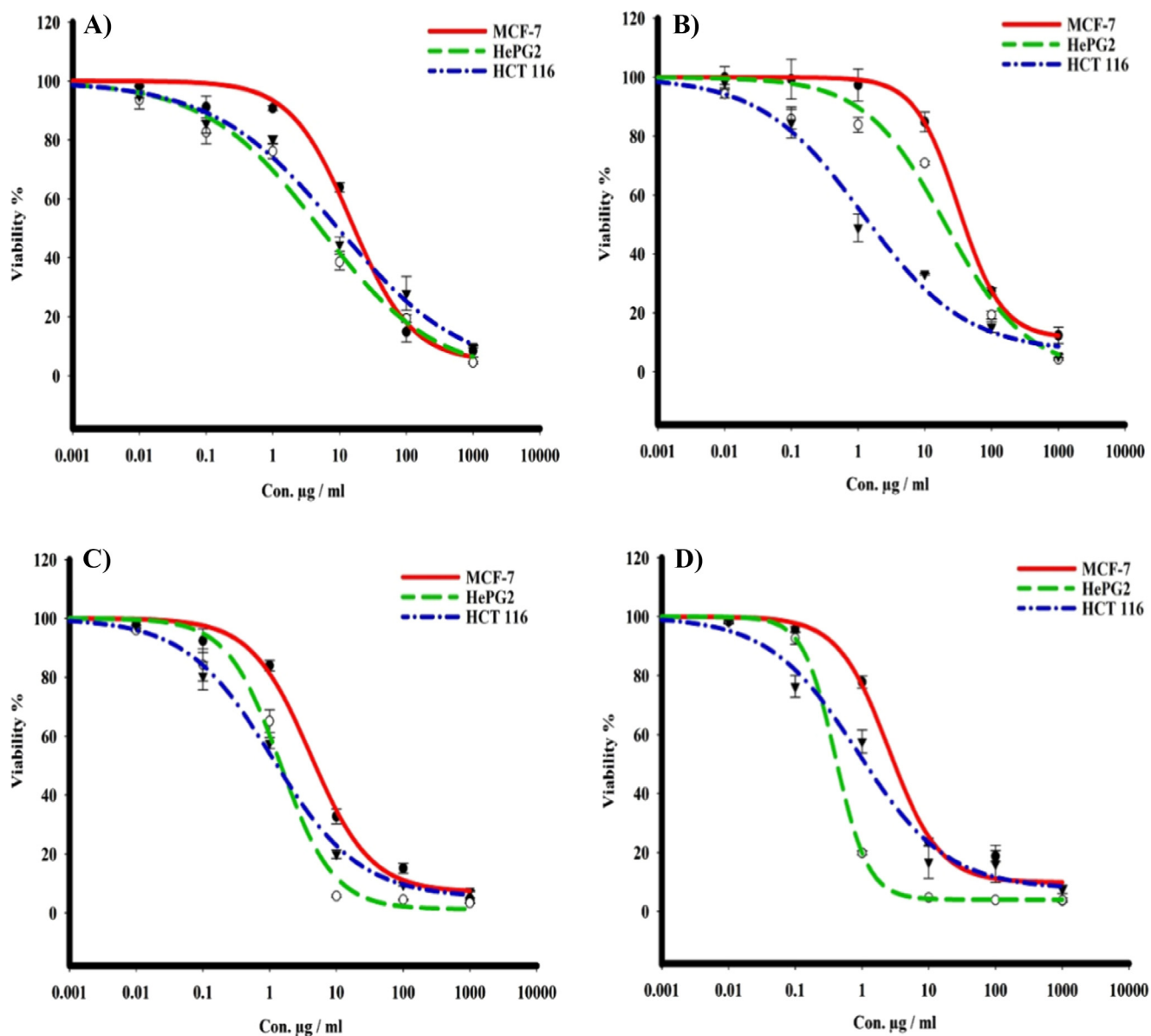


**Fig. 9** The dose response curves of the cytotoxicity of different compounds towards MCF-7, HepG2, and HCT 116 tumor cell lines. Cells were exposed to ligand and its metal complexes with different concentrations for 72 h. Cell viability was determined by SRB stain.

**Table 4** The  $IC_{50}$  ( $\mu\text{g}$ ) of the tested ligand and its metal complexes against different tumor cell lines.

Compound	$IC_{50}$ ( $\mu\text{g}$ )		
	MCF-7	HepG2	HCT 116
$C_{19}H_{15}ON_3$ ( $H_2L$ )	$17.6 \pm 1.5$	$5.7 \pm 0.5$	$10.2 \pm 1.3$
$C_{19}H_{14}ON_3ZrCl_3$	$45.6 \pm 0.9$	$21.6 \pm 1.1$	$1.6 \pm 0.2$
$C_{19}H_{14}ON_3CdCl$	$19.5 \pm 1$	$0.4 \pm 0.1$	$1.4 \pm 0.1$
$C_{19}H_{15}ON_3FeCl_3$	$5.1 \pm 0.4$	$1.1 \pm 1.4$	$1.3 \pm 0.2$

**Table 5** Biological activities of the ligand and its metal complexes against bacteria and fungus.

Compounds	Inhibition zone in mm		
	<i>A. niger</i>	<i>E. coli</i>	<i>B. subtilis</i>
DMSO	0	0	0
Nystatin	32	–	–
Tetracycline	–	35	38
<b>1</b>	25	30	32
<b>2</b>	22	19	26
<b>3</b>	29	30	32
<b>4</b>	24	19	15

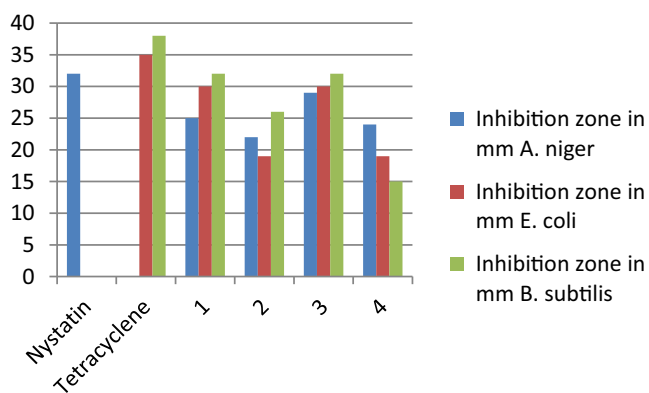


**Fig. 10** Evaluation of biological activities of the ligand and its metal complexes against bacteria and fungus.

hydroxynaphthylaldehyde was reported. The spectral data confirmed that the ligand adopted either a neutral tridentate or a monobasic tridentate mode, bonded to the metal ions

through the nitrogen atom of the heterocyclic benzimidazole, azomethine nitrogen atom and deprotonated phenolic oxygen atom forming either a square planer geometry. X-ray powder diffraction analysis of complexes indicated that the complexes are crystalline in structure with the triclinic system as well as having nan-sized dimensions. The antibacterial as well as the antifungal activities of the ligand and its complexes were evaluated against (*E. coli*), (*B. subtilis*) and *A. niger* by well-diffusion method. The results showed that cadmium (II) complex exhibited the highest antifungal activity and antibacterial activity among the tested complexes. The In vitro antitumor activities of different complexes were tested and the results revealed an important cytotoxicity of cadmium complex against MCF-7, Hep G2 and HCT 116 cell. Iron complex demonstrated also a strong toxicity towards Hep G2 and HCT cell but moderate activity against MCF-7. The bioassay study of the different complexes against mosquito larvae exhibited that Zr(IV) Complex showed significant activity with 0.172 values of LC50.

**Table 6** : Evaluation of the effectiveness of the insecticides used against the *Aedes aegypti* larvae, the vector of dengue fever in Makkah region.

Insecticide Used	Conc. (ppm)	Mortality (%) <sup>a</sup>	LC <sub>50</sub> (ppm) (LCL-UCL)	LC <sub>90</sub> (ppm) (LCL-UCL)	$\chi^2$ <sup>b</sup>	slope
C <sub>19</sub> H <sub>15</sub> ON <sub>3</sub> (H <sub>2</sub> L)	0.1	39.6	0.1717 (0.056–0.237)	0.9873 (0.77–3.939)	9.42	1.687
	0.3	59.4				
	0.5	74.0				
	0.8	85.4				
	1	96.6				
C <sub>19</sub> H <sub>14</sub> ON <sub>3</sub> ZrCl <sub>3</sub>	0.1	17.7	0.3093 (0.262–0.357)	1.372 (1.092–1.873)	2.2853	1.981
	0.3	49				
	0.5	62.5				
	0.8	77.1				
	1	88.5				
C <sub>19</sub> H <sub>14</sub> ON <sub>3</sub> CdCl	1	46.9	1.3356 (0.369–1.787)	7.6675 (5.665–26.548)	8.93	1.688
	3	63.5				
	5	82.3				
	8	89.6				
	10	97.9				
C <sub>19</sub> H <sub>15</sub> ON <sub>3</sub> FeCl <sub>3</sub>	1	21.9	3.6043 (2.986–4.278)	23.8079 (16.816–40.174)	3.2515	1.563
	3	39.6				
	5	59.4				
	8	67.7				
	10	80.2				

a: Five replicates, 20 larvae each.

b: Tabulated  $\chi^2 = 7.8$ , When tabulated  $\chi^2$  larger than calculated at 0.05 level of significance indicates the homogeneity of results.

**Table 7** Comparison between insecticides used against the *Aedes aegypti* larvae, on basis of LC<sub>50</sub> and resistance ratio values.

No	Line name	LC <sub>50</sub>	Lower limit	Upper limit	RR
1	C <sub>19</sub> H <sub>15</sub> ON <sub>3</sub> (H <sub>2</sub> L)	0.172	0.056	0.237	1
2	C <sub>19</sub> H <sub>14</sub> ON <sub>3</sub> ZrCl <sub>3</sub>	0.309	0.263	0.357	1.797
3	C <sub>19</sub> H <sub>14</sub> ON <sub>3</sub> CdCl	1.336	0.369	1.787	7.767
4	C <sub>19</sub> H <sub>15</sub> ON <sub>3</sub> FeCl <sub>3</sub>	3.604	2.986	4.277	20.953

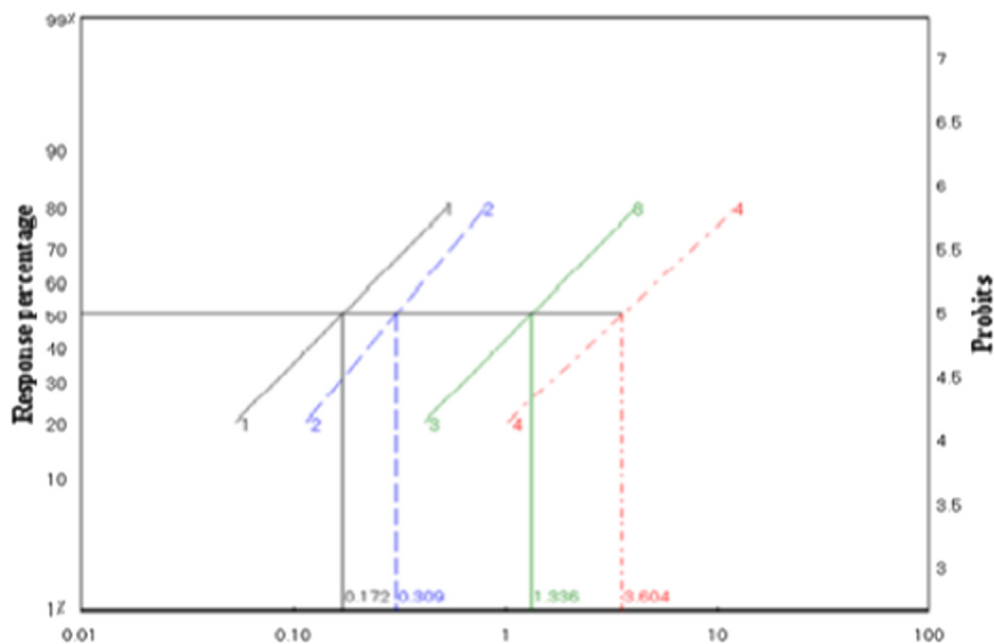


Fig. 11 Regression lines for insecticides used against the *Aedes aegypti* larvae using dipping technique.

#### Declaration of Competing Interest

The authors declare that they have no conflict of interest.

#### Acknowledgment

The authors extend their appreciation to the Department of Chemistry, College of Science, Qassim University and to the Deanship of Scientific Research at King Khalid University for funding this work through General Research Project under grant number (G.R.P-206-39).

#### References

- Abeer, A.T., Mohammed, M.A., Ahmed, M.R., Ahmed, A.E., 2015. Mixed Ligand Complex Formation of Cetirizine Drug with Bivalent Transition Metal (II) Ions in the Presence of 2-Aminomethylbenzimidazole: Synthesis, Structural, Biological, pH-Metric and Thermodynamic Studies. *J. Solution Chem.* 44, 1673–1704. <https://doi.org/10.1007/s10953-015-0362-9>.
- Abdulrahman, M.A., Hani, Z.A., Safwat, A.A., Ahmad, O.N., Ahmed, M.A., Mahmoud, A.E., Sameh, S.E., 2018. Anti-helicobacter, antitubercular and cytotoxic activities of scalaranes from the red sea sponge *hyrtios erectus*. *Molecules* 23, 978–989. <https://doi.org/10.3390/molecules23040978>.
- Abdul, A.R., Geetha, G.B., Saleem, G., Arumugam, S., Himalayan, B., 2000. Effect of *Feronia limonia* on mosquito larvae. *Fitoterapia* 71, 553–555. [https://doi.org/10.1016/S0367-326X\(00\)00164-7](https://doi.org/10.1016/S0367-326X(00)00164-7).
- Ahmed, A.E., 2011. Synthesis and characterization of some potential antitumor palladium (II) complexes of 2-aminomethylbenzimidazole and amino acids. *J. Coord. Chem.* 64, 2035–2055. <https://doi.org/10.1080/00958972.2011.587004>.
- Ahmed, N.A., 2020. Synthesis, Characterization and Microbicidal Activities of N-(hydroxy-4-((4-nitrophenyl)diazanyl)benzylidene)-2-(phenylamino)acetohydrazide metal complexes. *Egypt. J. Chem.* 63. <https://doi.org/10.21608/EJCHEM.2020.20906.2256>.
- Ali Mokhtar, M., Ahmed, M.A., David, A.L., Hany, A.E., 2012. Anti-cancer characteristics of mevinolin against three different solid tumor cell lines was not solely p53-dependent. *J. Enzyme Inhibition Med. Chem.* 27, 673–679. <https://doi.org/10.3109/14756366.2011.607446>.
- Arfa, K., Shamim, A., Maryam, A., Ghazala, H.R., Sohail, H., Sabahat, N., Jahan, Sarwat, Raheela, K., Hina, Z., 2015. Antimalarial and insecticidal activities of newly synthesized derivatives of Benzimidazole. *Pak. J. Pharm. Sci.* 28, 2179–2184.
- Balasubramanian, N., Deepika, S., Pradeep, K., 2012. Benzimidazole: a medicinally important heterocyclic moiety. *Med. Chem. Res.* 21, 269–283. <https://doi.org/10.1007/s00044-010-9533-9>.
- Chandrika, N.T., Sanjib, K.S., Huy, X.N., Sylvie, G.-T., 2016. Synthesis and investigation of novel benzimidazole derivatives as antifungal agents. *Bioorg. Med. Chem.* 24, 3680–3686. <https://doi.org/10.1016/j.bmc.2016.06.010>.
- Deepak, K., Rakesh, C., Dhamodaram, P., Balakrishnan, N., 2014. Larvicidal Activity of *Cassia occidentalis* (Linn.) against the Larvae of Bancroftian Filariasis Vector Mosquito *Culex quinquefasciatus*. *J. Parasit. Res.* 2014. <https://doi.org/10.1155/2014/236838>.
- El-Tabl, A.S., Fathey, A.E., Ahmed, N.A., 2008a. Spectroscopic characterization and biological activity of metal complexes with an ONO trifunctionalized hydrazone ligand. *J. Coord. Chem.* 61, 2380–2401. <https://doi.org/10.1080/00958970801914041>.
- El-Tabl, A.S., Fathey, A.E., Winfried, P., Ahmed, N.A., 2008b. Synthesis, spectroscopic characterization and biological activity of the metal complexes of the Schiff base derived from phenylaminoacetohydrazide and dibenzoylmethane. *Spectrochim. Acta Part A: Mol. Biomol. Spec.* 71, 90–99. <https://doi.org/10.1016/j.saa.2007.11.011>.
- Eman, D., Nader, A., Sandra, M., Daoyi, Li, Karim, El-B, Menna-Allah, S., Rawan, Al-K, Maha, N., Christian, K., Khaled, A., Mohamed, S., 2020. Development of benzimidazole-based derivatives as antimicrobial agents and their synergistic effect with colistin against gram-negative bacteria. *Eur. J. Med. Chem.* 186, 111850–111854. <https://doi.org/10.1016/j.ejmech.2019.111850>.
- Fahd, M.A., 2020. Synthesis, Design and Biological Evaluation of Antibacterial Activity of Novel Mixed Metal Complexes Derived from Benzimidazolphenylethanamine and 6-Amino-N, N-dimethyluracil. *Lett. Org. Chem.* 17. <https://doi.org/10.2174/1570178617666200210111442>.

- Fatma, G., Öztekin, A., Gökçen, E., Hatice, E., Nuran, D., Sibel, G., Aykut, Ö., 2003. Synthesis, cytotoxic activity on MCF-7 cell line and mutagenic activity of platinum (II) complexes with 2-substituted benzimidazole ligands. *Eur. J. Med. Chem.* 38, 473–480. [https://doi.org/10.1016/S0223-5234\(03\)00058-8](https://doi.org/10.1016/S0223-5234(03)00058-8).
- Gerald, J.C., Mackie, T.J., Mc Cartney, J.E., 1996. *Practical Medical Microbiology*. Churchill Livingstone, New York, p. 978.
- Gill, C., Ganesh, J., Mohammad, S., Rajesh, K., Anant, G., Deepak, N., Mahendra, S., 2008. Clubbed [1, 2, 3] triazoles by fluorine benzimidazole: a novel approach to H37Rv inhibitors as a potential treatment for tuberculosis. *Bioorg. Med. Chem. Lett.* 18, 6244–6247. <https://doi.org/10.1016/j.bmcl.2008.09.096>.
- Har, L.S., Jangbhadur, S., 2013. Synthesis of New Zirconium(IV) Complexes with Amino Acid Schiff Bases: Spectral, Molecular Modeling, and Fluorescence Studies. *J. Inorg. Chem. Inter.* <https://doi.org/10.1155/2013/847071>.
- Javaid, I., Faisal, I., Abdulaziz, S.A., Ayman, A.O., 2018. Evaluation of larvicidal efficacy of indigenous plant extracts against *Culex quinquefasciatus* (Say) under laboratory conditions. *Turk. J. Agricul. Forestry* 42, 207–215. <https://doi.org/10.3906/tar-1711-69>.
- Jeong-Chae, L., Hak-Ryul, K., Ju, K., Yong-Suk, J., 2002. Antioxidant property of an ethanolic extract of the stem of *Opuntia ficus-indica* var. *saboten*. *J. Agr. Food Chem.* 50, 6490–6496. <https://doi.org/10.1021/jf020388c>.
- Karelle, A., Jessica, B., Steven, S., Matthew, C., Domonique, W., Christian, F., Clifford, P., Colin, M., Debanjana, G., Shainaz, L., 2018. Nuclear magnetic resonance spectroscopy investigations of naphthalene-based 1, 2, 3-triazole systems for anion sensing. *Magnetochemistry* 4, 15–33. <https://doi.org/10.3390/magnetochemistry4010015>.
- Laugier, J., Bochu B., Chekcell: Graphical powder indexing cell and space group assignment software, 2004. <http://www.ccp14.ac.uk/tutorial/lmgp/achekcell.htm>.
- Leila, Z., Zeinab, F., Kamiar, Z., Fatemeh Bi Bi, M., Asghar, J., Soghra, K., 2020. Nano-SnCl<sub>4</sub>. SiO<sub>2</sub>, an efficient catalyst for synthesis of benzimidazole derivatives as antifungal and cytotoxic agents. *Res. Pharma. Sci.* 14, 504–514. <https://doi.org/10.4103/1735-5362.272536>.
- Lotfi, M.A., 2020. Novel Mixed Complexes Derived from Benzoimidazolphenylethanamine and 4-(Benzoimidazol-2-yl)aniline: Synthesis, characterization, antibacterial evaluation and theoretical prediction of toxicity, *Asian. J. Chem.* 32, 1266–1272. <https://doi.org/10.14233/ajchem.2020.22472>.
- Luo, Y., Xiao, F., Qian, S., Lu, W., Yang, B., 2011. Synthesis and in vitro cytotoxic evaluation of some thiazolylbenzimidazole derivatives. *Eur. J. Med. Chem.* 46, 417–422. <https://doi.org/10.1016/j.ejmech.2010.11.014>.
- Maghraby, M.T.-E., Ola, M.F.A., Samia, G.A., Asmaa, Y.A., Ola, I. A.S., 2020. Novel class of benzimidazole-thiazole hybrids: The privileged scaffolds of potent anti-inflammatory activity with dual inhibition of cyclooxygenase and 15-lipoxygenase enzymes. *Bioorg. Med. Chem.* 28, 115403–115413. <https://doi.org/10.1016/j.bmc.2020.115403>.
- Mauricio, C., Aline, M.L.Z., Queite, A.D.P., Marcela, B.P., Carla, C. O., Patriza, C., Maria, R.C., Ana Maria, D.C.F., 2019. Oxidative assets toward biomolecules and cytotoxicity of new oxindolimine-copper (II) and zinc (II) complexes. *Inorganics* 7, 12–29. <https://doi.org/10.3390/inorganics7020012>.
- Miranda, M.A.R., Sasaki, J.M., 2018. The limit of application of the Scherrer equation. *Acta Crystall Sect A: Found. Adv.* 74, 54–65. <https://doi.org/10.1107/S2053273317014929>.
- Monika, G., Singh, S., Mohan, C., 2014. Benzimidazole: An emerging scaffold for analgesic and anti-inflammatory agents. *Eur. J. Med. Chem.* 76, 494–505. <https://doi.org/10.1016/j.ejmech.2014.01.030>.
- Naeema, H.Y., Hoda, A.E., Mohamed, G., 2017. Synthesis, spectroscopic and DNA binding ability of CoII, NiII, CuII and ZnII complexes of Schiff base ligand (E)-1-(((1H-benzo [d] imidazol-2-yl) methylimino) methyl) naphthalen-2-ol. X-ray crystal structure determination of cobalt (II) complex. *Mat. Sci. Eng.: C* 75, 1059–1067. <https://doi.org/10.1016/j.msec.2017.02.171>.
- Neelam, B., Maurya, M.R., Fehmida, N., Amir, A., 2000. Synthesis and anti-moebic activity of new cyclooctadiene ruthenium (II) complexes with 2-acetylpyridine and benzimidazole derivatives. *Bioorg. Med. Chem. Lett.* 10, 2243–2245. [https://doi.org/10.1016/S0960-894X\(00\)00446-7](https://doi.org/10.1016/S0960-894X(00)00446-7).
- Patricia, T., Hugo, A.K., Bruno, P., Fernando, L., Aurélie, P., Christophe, B., Rodrigo, A., 2013. Organometallic benzimidazoles: Synthesis, characterization and antimalarial activity. *Inorg. Chem. Commun.* 35, 126–129. <https://doi.org/10.1016/j.inoche.2013.06.019>.
- Refaat, H.M., 2010. Synthesis and anticancer activity of some novel 2-substituted benzimidazole derivatives. *Eur. J. Med. Chem.* 45, 2949–2956. <https://doi.org/10.1016/j.ejmech.2010.03.022>.
- Rudolf, M., Virsinha, R., Aloysius, N., Fanuel, M., Dale, T., Nina, L., Lloyd, T., Marine, B., Charles, E., Bin, Z., Ravinder, R.K., Suresh, B.L., Matthias, R., Leslie, J.S., Kelly, C., 2020. Lerisetron Analogues with Antimalarial Properties: Synthesis, Structure-Activity Relationship Studies, and Biological Assessment. *ACS Omega* 5, 6967–6982. <https://doi.org/10.1021/acsomega.0c00327>.
- Rylands, L.-I., Athi, W., Keletso, M., Tameryn, S., Dale, T., Kelly, C., Gregory, S.S., 2019. Structure-activity relationship studies of antiplasmodial cyclometallated ruthenium (II), rhodium (III) and iridium (III) complexes of 2-phenylbenzimidazoles. *Eur. J. Med. Chem.* 161, 11–21. <https://doi.org/10.1016/j.ejmech.2018.10.019>.
- Sabrin, R.M.I., Hossam, M.A., Gamal, A.M., Samir, A.R., 2016. Integracides HJ: New tetracyclic triterpenoids from the endophytic fungus *Fusarium* sp. *Fitoterapia* 112, 161–167. <https://doi.org/10.1016/j.fitote.2016.06.002>.
- Samuel, T., John, K.R., Arivoli, S., 2012. Screening of twenty five plant extracts for larvicidal activity against *Culex quinquefasciatus* Say (Diptera: Culicidae). *Asian Pacific J. Tropical. Biomed.* 2, 1130–1134. [https://doi.org/10.1016/S2221-1691\(12\)60372-4](https://doi.org/10.1016/S2221-1691(12)60372-4).
- Shaharyar, M., Abdullah, M.M., Bakht, M.A., Majeed, J., 2010. Pyrazoline bearing benzimidazoles: search for anticancer agent. *Eur. J. Med. Chem.* 45, 114–119. <https://doi.org/10.1016/j.ejmech.2009.09.032>.
- Singh T. B., Rey L., Gartia R. Applications of PeakFit software in thermoluminescence studies, 2011. <http://noir.niscair.res.in/handle/123456789/11596>.
- Ülku, Y., Suat, T., Nesrin, B., Kemal, Y., Küçükbay, Hasan, Suleyman, S., 2019. Synthesis and evaluation of anticancer properties of novel benzimidazole ligand and their cobalt (II) and zinc (II) complexes against cancer cell lines A-2780 and DU-145. *Inorg. Chimica Acta* 495, 118977–118983. <https://doi.org/10.1016/j.ica.2019.118977>.
- Vatsal, P., Navin, P., Manuel, C.-B., Gildardo, R., 2020. N-Mannich bases of benzimidazole as a potent antitubercular and antiprotozoal agents: Their synthesis and computational studies. *Synt. Commun.* 50, 858–878. <https://doi.org/10.1080/00397911.2020.1725057>.
- Wang, X.J., Mei, Y.X., Ji, H.F., Fu, R.Z., Gui, F.C., Qi, D.Y., 2012. Synthesis, biological evaluation and SAR studies of benzimidazole derivatives as H1-antihistamine agents. *Chin. Chem. Lett.* 23, 707–710. <https://doi.org/10.1016/j.ccl.2012.04.020>.
- Yadav, S., Narasimhan, B., Kaur, H., 2016. Perspectives of Benzimidazole Derivatives as Anticancer Agents in the New Era. *Anti-cancer Agents Med. Chem.* 16, 1403–1425.
- Ying, L., Liping, L., Miolu, Z., Qingming, W., Caixia, Y., Shu, X., Xueqi, F., Yuhua, M., 2011. Potent inhibition of protein tyrosine phosphatases by copper complexes with multi-benzimidazole derivatives. *Biometals* 24, 993–1004. <https://doi.org/10.1007/s10534-011-9460-3>.